IOP PUBLISHING JOURNAL OF PHYSICS: CONDENSED MATTER

J. Phys.: Condens. Matter **20** (2008) 365221 (6pp) doi:10.1088/0953-8984/20/36/365221

Vibrational effects on $SrTiO_3$ Ti 1s absorption spectra studied using first-principles methods

Silvia Tinte[1,3] **and Eric L Shirley**[2]

[1] Ceramics Division, National Institute of Standards and Technology, 100 Bureau Drive, Stop 8520, Gaithersburg, MD 20899-8520, USA
[2] Optical Technology Division, National Institute of Standards and Technology, 100 Bureau Drive, Stop 8441, Gaithersburg, MD 20899-8441, USA

Received 20 May 2008, in final form 21 July 2008
Published 20 August 2008
Online at stacks.iop.org/JPhysCM/20/365221

Abstract

We analyze the vibrational effects on the Ti 1s excited states in cubic $SrTiO_3$ and related pre-edge x-ray absorption fine structure using first-principles methods. Ground-state, total-energy and electron–core hole Bethe–Salpeter calculations are performed for different atomic configurations related to e_g-symmetry distortions of $SrTiO_3$. From these, we can obtain normal-mode gradients of the electronic excited-state energy, i.e., of the excited-state Born–Oppenheimer surface. This yields the corresponding electron–phonon coupling coefficients that allow us to predict the spectral broadening induced by those vibrational modes.

(Some figures in this article are in colour only in the electronic version)

1. Introduction

The excitation spectra of molecules and solids depend on the electronic and vibrational degrees of freedom. Hence, their complete description must reflect both of the above. For instance, the pre-edge features in the Ti 1s edge in a perovskite compound reflect the crystal field-split 3d manifold, but each peak is itself broadened for several reasons, including lattice vibrations. Nowadays, core and valence-electron excitations and spectra are often calculated using the Bethe–Salpeter equation (BSE). However, this is usually done for fixed atomic positions. Beyond that, the spectra can be calculated using the Born–Oppenheimer approximation, so that the electronic and nuclear motions are considered independently. In this approximation, the electronic energy is treated as a function of atomic configurations around some equilibrium one. Initially, when an electron–hole pair is created by optical excitation, the final state has approximately the same atomic configuration as the initial state. However, optical transitions such as occur in x-ray absorption formally involve electronic-vibrational levels. As a result, vibrational effects shift and broaden spectral features because of coupling of atomic displacements to electronic states and excitations.

[3] Present address: Instituto de Desarrollo Tecnológico para la Industria Química (INTEC), Güemes 3450, 3000 Santa Fe, Argentina.

In this work we compute the electronic excited-state forces in order to include the vibrational effects on the spectrum for the Ti K-shell electron excitation spectra in cubic $SrTiO_3$ (STO). The Ti K near-edge absorption spectrum is characterized by Ti 1s–3d quadrupolar transitions, to the lower, triply-degenerate T_{2g} (d_{xy}, d_{yz}, d_{zx}) state and upper, doubly-degenerate E_g ($d_{x^2-y^2}$, $d_{3z^2-r^2}$) state. In the presence of the attractive potential of a Ti 1s core hole, such states are essentially localized molecular orbitals. The forces are computed within the Born–Oppenheimer approximation. By combining these results with those of vibrational-mode calculations and going beyond the Born–Oppenheimer approximation using a model Hamiltonian, we incorporate key vibrational effects into the absorption spectrum.

Section 2 describes vibrational-mode (phonon) calculations in cubic STO (in the electronic ground state). In section 3, we present an approximation that we use to calculate excited-state forces in the case of core excitations. Section 4 gives the results for our calculated spectra and Born–Oppenheimer excited-state energy in cubic STO with the atoms displaced along localized vibrational e_g modes. In section 5 we describe the model Hamiltonian used to quantify the broadening of the electronic excitation spectrum resulting from such vibrational degrees of freedom.

Table 1. Irreducible representations (irr. rep.) and calculated wavenumbers (ν/c) for Γ-point phonons in cubic STO.

irr. rep.	ν/c (cm^{-1})
t_{1g}	$113i$
t_{1u}	99, 187, 454, 587
t_{2g}	136, 433
t_{2u}	221
e_g	545
a_{1g}	887

2. Phonon calculations

$SrTiO_3$, one of the best-studied perovskite materials, adopts the centrosymmetric cubic structure at room temperature, and undergoes a structural phase transition from the cubic to a tetragonal, nonpolar antiferrodistortive (AFD) phase as the temperature drops below 105 K [1, 2]. Cooling to still lower temperatures results in a strong Curie–Weiss-type increase in the static dielectric response, suggestive of a phase transition at about 36 K. However, no ferroelectric transition actually occurs, and the dielectric constant saturates to an enormous value at zero temperature.

First-principles calculations have contributed significantly to the understanding of the structural properties of STO. In particular phonon calculations in cubic STO at the zero-wavevector Γ point are well reported in the literature [3, 4], as well as in the tetragonal phase [5]. Because we want to analyze vibrational effects involving the six oxygen atoms around one Ti, we report phonon calculations using a doubled unit cell with the two Ti atoms along the [111] direction. First-principles, density functional [6] calculations were performed within the local-density approximation (LDA) [7] as implemented in the ABINIT code [8][4]. Teter extended-norm-conserving pseudopotentials [9] were used treating 10 electrons as valence for $Sr(4s^24p^65s^2)$, 12 for $Ti(3s^23p^64s^23d^2)$ and 6 for $O(2s^22p^4)$. Calculations were performed with a $6 \times 6 \times 6$ Monkhorst–Pack **k**-point mesh [10]. The electronic wavefunctions were expanded in a plane-wave basis up to 100 Ryd. Our calculations were carried out at the resulting theoretical cubic lattice constant of 3.845 Å, which is about 1.3% smaller than the experimental value of 3.897 Å extrapolated to 0 K, in agreement with the typical LDA underestimation found in previous studies. Table 1 shows the phonon wavenumbers for the various irreducible representations. The imaginary frequency of the t_{1g} mode, which involves octahedron rotation, indicates an AFD instability at our particular LDA lattice parameter, while the first t_{1u} mode corresponding to the ferroelectric (FE) distortion is stable. Our results are in good agreement with previous theoretical [5] and experimental results [11]. However, there are small differences among the lattice parameter values used that affect the vibrational frequencies, consistent with the structural instabilities in FE perovskites being strongly dependent on the unit cell volume.

[4] Certain commercial products are identified in this work for purposes of clarity. Mention of such products does not constitute an endorsement by the National Institute of Standards and Technology and does not indicate that they are necessarily the best products for a given purpose.

From symmetry analysis, one can identify the modes that can directly affect the Ti 3d orbitals through Jahn–Teller distortions. We focus therefore on even-parity modes that mainly involve change of the Ti–O bond length, such as the a_{1g} breathing mode and the e_g modes, as opposed to the t_{1g} octahedron-rotation modes and t_{2g} distortion modes. In relation to Ti 1s-to-3d excitations, we specifically analyze the local oxygen-octahedron vibrational effects, and so seek to obtain the corresponding frequency spectra. For this purpose, we borrow the short-range, 'local-mode' O–O interatomic force constants (IFC) from [12] computed for $BaTiO_3$ and $PbTiO_3$ and solve the constrained normal-mode problem to obtain the frequencies. Our use of these IFCs for STO is justified by the fact that they are almost independent of the A (and, to a lesser degree B) sites in ABO_3 perovskites.

For completeness, one should consider the sensitivity of the present results to the choice of density functional (LDA in this case). Tinte *et al* [13] found that use of a generalized-gradient approximation (GGA) overestimates the theoretical volume in STO and hardens the phonon frequencies as compared to the LDA ones at the experimental volume. In particular, the GGA stabilizes STO against ferroelectric distortions. More recent electronic-structure calculations in perovskites render similar results for a wide variety of properties in the LDA and within a given GGA [14, 15]. Anyhow that does not affect the present results. Indeed, the high-frequency e_g local-mode oscillator should be qualitatively unchanged when comparing LDA and GGA calculations. We also expect that other aspects of the choice of density functional that is used, including local dielectric screening effects, should be robust with respect to that choice. These screening effects describe how the charge density is affected by a Ti 1s core hole and its concomitant potential disturbance.

Use of a functional like LDA + U [16], as compared to the LDA, is not critical in the present study of STO. There is nominally at most one 3d orbital occupied on the Ti site, and this occurs only within the Bethe–Salpeter calculations, where an electron does not have the self-interaction that typically plagues LDA studies involving transition-metal and rare-earth systems. However, it is clear that the present Bethe–Salpeter approach will not work as well when there is a partially-filled d or f shell in the ground state or when a system is strongly correlated [17]. In such situations, it can be important to use methods like LDA + U in ground-state calculations, perhaps in combination with approaches such as dynamical mean-field theory (DMFT) in order to better treat strong correlation and multiply-excited many-body states [18].

3. Excited-state forces

When an electron is excited from a core level in a solid, it leaves behind a core hole. The x-ray extinction coefficient can be given by the expression, $\mu(\varepsilon) \sim -\mathrm{Im}\langle 0|O[\varepsilon + \mathrm{i}\gamma(\varepsilon) - H]^{-1}|0\rangle$. This involves the electronic ground-state $|0\rangle$, light–matter interaction O, and core-excited Hamiltonian H. H includes realistic descriptions of electron core and band states, as well as the electron–core hole interaction screened in a self-consistent fashion [17, 19]. Here $\mu(\varepsilon)$ for excitation energy ε is calculated by solving the Bethe–Salpeter equation (BSE),

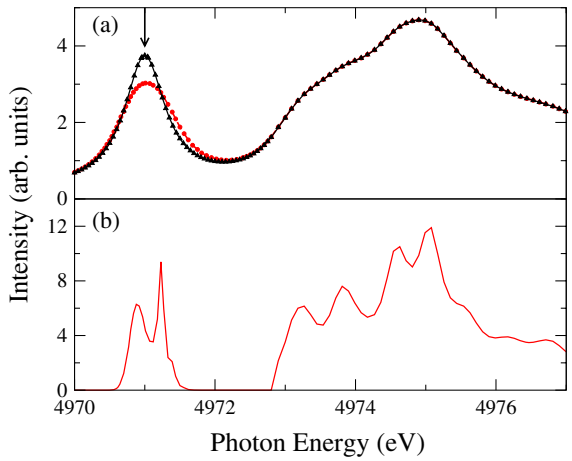

Figure 1. Calculated Ti K spectra for cubic $SrTiO_3$. The top panels shows spectra with all broadening effects except vibrational ones (line with points) and all broadening effects (points). The bottom panel shows a spectrum that includes vibrational broadening from the model Hamiltonian around the E_g peak and a minimal degree of other broadening effects for presentation purposes. The arrow shows the center-of-mass of the E_g peak's spectral weight.

which is the coupled equation of motion for the interacting electron–hole pair. The parameter $\gamma(\varepsilon)$ is included to account for experimental resolution, core hole lifetime broadening and intrinsic broadening of the electron band states that are typically probed at a given excitation energy [22].

The excited-state total energy of the system in a given atomic configuration specified by atomic coordinates Q is

$$E^*_{\rm tot}(Q) = E_0(Q) + \Delta E_{\rm el}(Q). \quad (1)$$

This is the sum of the atom-configuration-dependent electronic ground-state LDA total energy, $E_0(Q)$, and the change of electronic energy between the final and initial state, $\Delta E_{\rm el}(Q)$. Thus, $E_0(Q)$ describes the shape of the ground-state Born–Oppenheimer surface versus Q, whereas $\Delta E_{\rm el}(Q)$ describes the vertical separation of the ground- and excited-state surfaces as a function of Q:

$$\Delta E_{\rm el}(Q) = [E_{\rm CBM}(Q) - E_{\rm B}(Q)] - E_{\rm C}(Q). \quad (2)$$

This involves the 3d binding energy, $E_{\rm B}(Q)$, given by the first peak of the calculated absorption spectrum relative to the conduction-band minimum, $E_{\rm CBM}(Q)$. The initial-state energy is the relative 1s binding energy, $E_{\rm C}(Q)$. For this, we use the approximation

$$E_{\rm C}(Q) = C + E^{\rm LDA}_{\rm local}(Q) + [\Delta W_c(Q) - \Delta V_c]/2, \quad (3)$$

where $E^{\rm LDA}_{\rm local}(Q)$ is the local Hartree plus exchange/correlation potential at a Ti site obtained from the electronic ground-state LDA calculations, and the $[\Delta W_c(Q) - \Delta V_c]/2$ term accounts for the valence electrons' contribution to the screening of the core hole potential as described in [19]. Division by two arises for familiar reasons related to linear-response arguments. C is a large additive constant accounting for the remainder of the Ti 1s binding energy. In this way we estimate the core-level binding energy in a manner different from the formalism

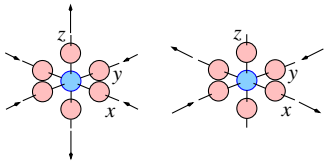

Figure 2. Vibration e_g modes, which we dub $e_{g,3z^2-r^2}$ (left) and e_{g,x^2-y^2} (right).

presented in [20] where the valence-hole binding energy is computed using other approximations more appropriate to the valence case.

We explore the excited-state Born–Oppenheimer surface along selected directions that correspond to atomic configurations with displaced atoms following selected vibrational modes. The e_g modes appear to affect spectra by far the most strongly, and we henceforth consider them only. While distortion along the a_{1g} mode directly affects the various terms in $\Delta E_{\rm el}(Q)$ strongly, the effects appear to cancel. For several configurations along the e_g mode directions, we compute $E^*_{\rm tot}(Q)$. The derivatives of $E^*_{\rm tot}(Q)$ with respect to the mode amplitudes give the excited-state forces. For the BSE calculations, we use norm-conserving pseudopotentials with Ti 3s/3p/3d, Sr 4s/4p/4d, and O 2s/2p/3d states treated as valence states and an 81 Ryd plane-wave cutoff. The full Brillouin zone is sampled at 512 **k**-points, which is well converged. About 60 conduction bands are included when calculating spectra. As in the earlier section, we use a 10 atom supercell with two primitive units displaced along the [111] direction with local oxygens displaced oppositely. We assume the room temperature experimental lattice constant of 3.905 Å. Further details are provided in [21].

4. Results

For cubic STO, figure 1 shows calculated x-ray absorption spectra for excitation near the Ti K edge, assuming a 4971 eV separation between the Ti 1s level and conduction-band minimum. We consider two equivalent combinations of incident x-ray radiation propagation direction, $\hat{q}$, and x-ray electric-field direction, $\hat{e}$: (1) $\hat{q} \parallel 110$, $\hat{e} \parallel 1\bar{1}0$, and (2) $\hat{q} \parallel 101$, $\hat{e} \parallel 10\bar{1}$. These combinations both allow quadrupolar transitions of the Ti 1s electrons to the Ti 3d-derived E_g unoccupied molecular orbitals. Three calculations are shown. In panel (a), there is a spectrum that includes only the broadening because of $\gamma(\varepsilon)$, using a black line, in which the arrow indicates the peak position before broadening. In panel (b), there is a spectrum with only the vibrational broadening of the E_g peak. We obtained this broadening with the model Hamiltonian described in section 5. However, the γ-broadened version of the full spectrum including the vibration broadening is also shown using a red line in panel (a). The vibrational broadening leads to a smaller peak height and larger peak width, but is less pronounced when viewed in combination with broadening because of $\gamma(\varepsilon)$. The experimental spectrum has been presented by Woicik *et al* [21].

When the six nearest oxygen atoms are displaced following the $e_{g,3z^2-r^2}$ and e_{g,x^2-y^2} vibrational modes (see figure 2), the E_g peak varies as indicated in figures 3 and 4.

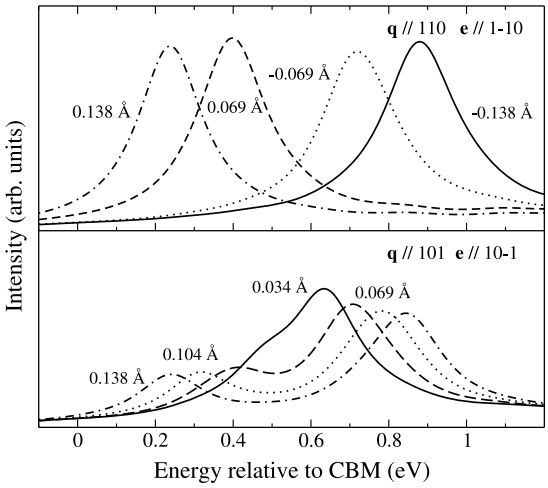

Figure 3. Electronic E_g-derived peaks for distorted configurations following the vibrational $e_{g,3z^2-r^2}$ mode.

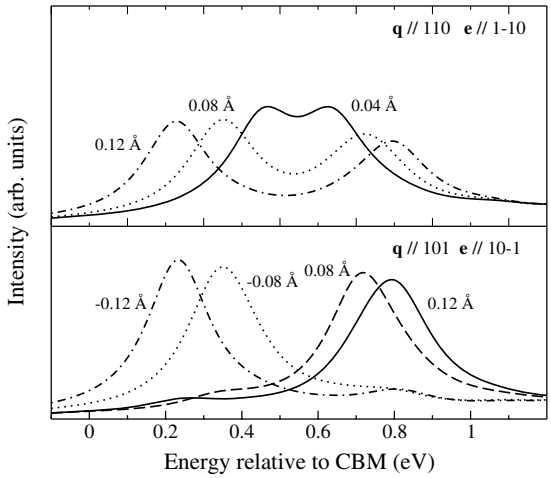

Figure 4. Electronic E_g-derived peaks for distorted configurations following the vibrational e_{g,x^2-y^2} mode.

In the $e_{g,3z^2-r^2}$ mode, the apical oxygens move twice as much as the in-plane ones, and there is a relative sign difference for changes in the apical versus in-plane Ti–O distance. In the e_{g,x^2-y^2} mode, the four in-plane oxygens move along the x versus y directions inward or outward by equal but opposite amounts. For normalized displacement patterns, the mode amplitude is a scalar that can be represented by Q_θ and Q_ε for $e_{g,3z^2-r^2}$ and e_{g,x^2-y^2}, respectively, following the notation of [23]. Figure 3 (figure 4) shows the calculated spectra for distorted configurations following the $e_{g,3z^2-r^2}$ (e_{g,x^2-y^2}) mode for different displacement amplitudes. Undistorted cubic STO corresponds to $Q_\theta = Q_\varepsilon = 0$. When an e_g distortion of the TiO_6 octahedron is imposed, the degeneracy of the E_g-derived electronic states is lifted. The new singly-degenerate states have symmetries that depend on the distortion. For a given $\hat{q}$ and $\hat{e}$, the associated quadrupole-transition moments determine the peak heights. As a check, we confirmed that geometrical analysis predicts relative peak heights like those shown in figures 3 and 4.

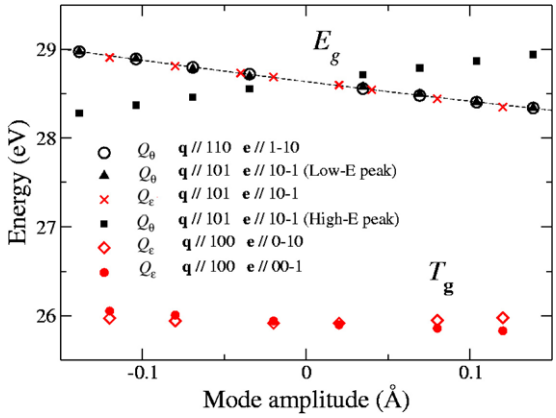

Figure 5. Excited-state Born–Oppenheimer surface along the vibrational e_g modes for different $\hat{q}$ and $\hat{e}$ directions.

There is only one parameter necessary to describe the E–e electronic-vibrational coupling. Using the peak positions and the results of performing LDA total energy and valence-electron screening calculations, we obtain $E^*_{\rm tot}(Q)$ for each configuration as described in section 3. We have also analyzed spectra for the combinations, $\hat{q} \parallel 100$, $\hat{e} \parallel 010$, and $\hat{q} \parallel 100$, $\hat{e} \parallel 001$. From this analysis we can observe how Ti 1s–3d T_{2g} transitions are affected by the e_g modes. All excited-state total-energy curves as a function of e_g mode amplitudes are plotted in figure 5, as such curves can be deduced from the apparent positions of pre-edge absorption features.

Fitting the energy curve with a quadratic expansion in the mode amplitude, for the E_g peaks we obtain a slope of $F = -2.3$ eV Å^{-1} evaluated at zero displacement. For the T_{2g} peaks, the energy curve is comparatively flat in the same amplitude range, so we can neglect the e_g-mode vibrational effects on the T_{2g} peaks and only consider the electronic E_g states. This also leaves untreated the Ti–O_6 relative displacement, which can allow Ti 3d–4p hybridization and strongly affect the spectrum [21].

5. Model Hamiltonian

To determine the vibration effects on spectra, we solve a Hamiltonian that includes an electronic term accounting for the E_g core hole exciton states, a vibrational term that describes the e_g vibrational Hamiltonian, and a coupling term between the excitonic and vibrational states. This phenomenon is described by the Jahn–Teller theorem[5]. As already noted, structural distortions away from the cubic-symmetry $Q = 0$ nuclear configuration along the degenerate normal-mode coordinates remove the degeneracy of core hole exciton levels. In particular, the E–e Jahn–Teller problem [23, 24] is one of the relatively simple cases that can be solved analytically in the weak- and strong-coupling limits (i.e., small-F and large-F). In this case, the coupling is of intermediate strength, so a numerical solution is best. Hence, we briefly summarize how one numerically solves the Jahn–Teller problem, which

[5] The Jahn–Teller theorem states that, if a system has a spatially degenerate electronic state and other appropriate conditions apply, the system will distort in such a way as to remove the electronic degeneracy.

is already well described elsewhere [23], and then present our results.

In general, to solve a Jahn–Teller problem one can first find the active coordinates or space of possible distortions Q for the given f-fold degenerate electronic manifold. For each state k in the manifold, the electronic wavefunction is $\xi_k(r, Q)$, where r indicates the electronic degrees of freedom. Here, k can have one of two values, which we denote by the symmetry of the core hole exciton wavefunction, $k = 3z^2 - r^2$ or $k = x^2 - y^2$. The system's full dynamics involve a wavefunction $\Psi(r, Q) = \sum_k \chi_k(Q)\xi_k(r, Q)$. The expansion coefficients $\{\chi_k(Q)\}$ depend only on Q. The electronic wavefunction $\xi_k(r, Q)$ is also Q-dependent. This was included automatically in our BSE calculations, but to simplify the model Hamiltonian, we assume $\xi_k(r, Q) = \xi_k(r, 0)$. We can then solve f (in this case, $f = 2$) coupled equations of the form

$$[\Delta E_{\rm el}(Q = 0) + H_Q + E_{\rm vib}(Q) - E]\chi_k(Q) + \sum_{k'} W_{kk'}(Q)\chi_{k'}(Q) = 0. \quad (4)$$

H_Q represents the kinetic energy of the TiO_6 cage oxygen nuclei, and $E_{\rm vib}(Q)$ is the quadratic vibrational term that describes the restoring force for the e_g vibrational modes. In the Ti 1s core hole excited state with the electron in the E_g manifold of 3d states, $W_{kk'}(Q)$ describes the electronic-vibrational coupling that modifies the shape of the E_g peak. For small values of Q, we have

$$W_{3z^2-r^2,3z^2-r^2} \approx FQ_\theta, \quad (5)$$

$$W_{x^2-y^2,x^2-y^2} \approx -FQ_\theta, \quad (6)$$

and

$$W_{3z^2-r^2,x^2-y^2} = W_{x^2-y^2,3z^2-r^2} \approx -FQ_\epsilon. \quad (7)$$

Retaining only this linear term is referred to as the E–e problem.

The resulting coupled equations for this E–e problem have an underlying symmetry, which ensures that the vibrationally broadened spectrum is the same for any linear combination of E_g core-excited states produced according to a combination of $\hat{q}$ and $\hat{e}$. Physically, the equations describe two equivalent vibrational oscillators coupled to an otherwise doubly-degenerate core hole excitonic system. They have known analytical solutions only in the limiting cases of weak and strong coupling, defined using the dimensionless ratio, $E_{\rm JT}/(\hbar\omega)$. For the linear E–e problem, the Jahn–Teller energy $E_{\rm JT}$ is defined as $E_{\rm JT} = F^2/(2\mu\omega^2)$, where μ is the oxygen ion mass. The values of F and ω documented in previous sections imply $E_{\rm JT} = 0.6158$ eV and $\hbar\omega = 0.0335$ eV. Elegant methods for numerical solution of equation (4) and resulting spectra have been formulated [23, 24]. We have used such methods and also confirmed their results by our own numerical calculations using the Haydock recursion method without exploiting symmetry to the same degree.

Figure 1(b) shows the energy spread of the E_g peak only because of vibrational effects. However, figure 1(a) shows that, once experimental and electronic lifetime widths are included (with the black curve including only these effects), the vibrational effects on the spectrum are less perceptible (with the points including these effects as well). Thus, this work quantifies vibrational effects and suggests that, for the Ti 1s edge, the Jahn–Teller E–e broadening of the E_g peak is at most weakly discerned.

6. Conclusion

In this work, we have used results obtained by others and carried out our own calculations related to vibrational properties of perovskites, the electron–core hole Bethe–Salpeter equation, x-ray absorption spectroscopy, electronic-vibrational coupling, and the E–e Jahn–Teller problem. These findings have all been applied to the broadening of the E_g peak in the Ti 1s near-edge spectrum in $SrTiO_3$, though the results should also be of interest for many other compounds. While there is significant broadening of the E_g peak because of E–e Jahn–Teller coupling, other broadening effects can obfuscate this.

The role of the same Jahn–Teller coupling in the context of a Ti L-edge calculation could be of particular interest, because one has a smaller core hole width to consider and the added complication of significant multiplet effects. It should not be difficult to include all such effects and the vibrational effects in a calculation that would differ from a measured absorption spectrum chiefly because of the effects of multi-electron excitations. Furthermore, the T_{1u} ferroelectric distortions involving the Ti being displaced with respect to the O_6 cage also remain to be considered in the case of the Ti 1s edge, where 3d–4p hybridization can greatly enhance the relatively large dipole character of the hybridized E_g peak.

References

[1] Fleury P A, Scott J F and Worlock J M 1968 *Phys. Rev. Lett.* **21** 16
[2] Uwe H and Sakudo T 1976 *Phys. Rev.* B **13** 271
[3] Lasota C, Wang C-Z, Yu R and Krakauer H 1997 *Ferroelectrics* **194** 109
[4] Antons A, Neaton J B, Rabe K M and Vanderbilt D 2005 *Phys. Rev.* B **71** 024102
[5] Sai N and Vanderbilt D 2000 *Phys. Rev.* B **62** 13942
[6] Hohenberg P and Kohn W 1964 *Phys. Rev.* **136** B864
[7] Kohn W and Sham L J 1965 *Phys. Rev.* **140** A1133
[8] Gonze X *et al* 2002 *Comput. Mater. Sci.* **25** 478–492
Gonze X *et al* 2005 *Z. Kristallogr.* **220** 558–62
[9] Teter M 1993 *Phys. Rev.* B **48** 5031
[10] Monkhorst H J and Pack J D 1976 *Phys. Rev.* B **13** 5188
[11] Servoin J L, Lusoin Y and Gervais F 1980 *Phys. Rev.* B **22** 5501
[12] Ghosez Ph, Cockayne E, Waghmare U V and Rabe K M 1999 *Phys. Rev.* B **60** 836
[13] Tinte S, Stachiotti M G, Rodriguez C O, Novikov D L and Christensen N E 1998 *Phys. Rev.* B **58** 11959
[14] Bilc D I, Orlando R, Shaltaf R, Rignanese G-M, Íñiguez J and Ghosez Ph 2008 *Phys. Rev.* B **77** 165107
[15] Rodriguez J A, Etxeberria A, González L and Maiti A 2002 *J. Chem. Phys.* **117** 2699
[16] Anisimov V I, Zaanen J and Anderseon O K 1991 *Phys. Rev.* B **44** 943
[17] Shirley E L 2005 *J. Electron Spectrosc. Relat. Phenom.* **144** 1187

[18] Kotliar G, Savrasov S Y, Haule K, Oudovenko V S, Parcollet O and Marianetti C A 2006 *Rev. Mod. Phys.* **78** 865
[19] Shirley E L 2006 *Ultramicroscopy* **106** 986
[20] Ismail-Beigi S and Louie S G 2003 *Phys. Rev. Lett.* **90** 076401
[21] Woicik J C, Shirley E L, Hellberg S C, Andersen K E, Sambasivan S, Fischer D A, Chapman B D, Stern E A, Ryan P, Ederer D L and Li H 2007 *Phys. Rev.* B **75** 140103(R)
[22] Shirley E L, Soininen J A and Rehr J J, unpublished
[23] Bersuker I B and Polinger V Z 1989 *Vibronic Interactions in Molecules and Crystals* (Berlin: Springer)
[24] Longuet-Higgins H C, Öpik U, Pryce M H L and Sack R A 1958 *Proc. R. Soc.* A **244** 1